Journal of Solid State Chemistry **144,** 392–397 (1999)
Article ID jssc.1999.8177, available online at http://www.idealibrary.com on IDEAL®

Some Features of the Reduction Process from $CrVO_4$ to $CrVO_3$

Irma L. Botto,* Marta B. Vassallo,* Manlio Occhiuzzi,† Dante Cordischi,† and Piero Porta†,[1]

*Química Inorgánica (CEQUINOR), Facultad de Ciencias Exactas, Universidad Nacional de La Plata, 1900 La Plata, Argentina; and
†Centro del Consiglio Nazionale delle Ricerche su Struttura e Attività Catalitica di Sistemi di Ossidi (SACSO), Dipartimento di Chimica, Università La Sapienza, Piazzale Aldo Moro 5, 00185 Rome, Italy

Received November 12, 1998; in revised form December 20, 1998; accepted December 22, 1998

The reduction process from $CrVO_4$ to $CrVO_3$ was investigated by temperature programmed reduction; thermogravimetry; XRD, IR, and ESR spectroscopies; and SEM microscopy. This detailed analysis shows that the corundum-type $CrVO_3$ mixed oxide forms from 900 K and suggests as an intermediate stage the incorporation of Cr^{III} in a VO_2 rutile type phase. The absence of the V_2O_3 typical free-carrier behavior could result from the Cr^{III} in the lattice and it is clearly revealed by IR spectroscopy.

Key Words: **TPR; IR spectroscopy; chromium vanadates.**

INTRODUCTION

$CrVO_4$ is a very interesting material widely used as an oxidation catalyst in some important industrial reactions including oxidation of benzene to maleic anhydride or methanol to formaldehyde (1). The reduction of V^V leads to the formation of the $CrVO_3$ mixed oxide at high temperature ($\sim$ 1200 K) in H_2 atmosphere (2). $CrVO_3$ is a member of the $(V_{1-x}Cr_x)_2O_3$ solid solution where α-V_2O_3 and α-Cr_2O_3 are the final members of the series. All these oxides adopt the corundum type structure (hexagonal symmetry, space group $R\bar{3}c$ with a V- and Cr-octahedral coordination (2, 3).

α-Cr_2O_3 is an antiferromagnetic insulator with a Neel temperature (T_N) of 308 K, while α-V_2O_3 is a metallic conductor at room temperature and is transformed into a semiconducting monoclinic phase at 150–160 K (2). Suggestively, doping with Cr induces metal insulator transition in V_2O_3 without change in the lattice symmetry, although it greatly reduces the c/a ratio of the corundum structure (2, 4).

The structure of V_2O_3 and of some other low oxides, for example V, Mo, W oxides, typically shows a strong metal–metal interaction. This is consistent with the shorter V–V bond length and it is also related to the octahedra sharing edges and the free electrons available per bond (5). The presence of a metal with valence electrons that are not engaged in metal oxygen bonding implies a possible magnetic coupling effect. In general, the insulating phases of this system exhibit relatively large separations among nearest-neighboring vanadium ions, disrupting the conduction band structure (6).

This paper reports the analysis of the reduction process of the $CrVO_4$ phase by temperature programmed reduction (TPR), thermogravimetry (TG) and XRD techniques, IR and ESR spectroscopies, and SEM microscopy. The analysis of V_2O_5 TPR pattern is included as reference. We also investigated the effect of the Cr atoms on the strong V–V interaction observed in the V_2O_3 by IR spectroscopy. Finally, we studied the reverse reaction, from $CrVO_3$ to $CrVO_4$, focusing our interest on the intermediate reduction step.

EXPERIMENTAL

$CrVO_4$ was obtained by solid state reaction between V_2O_5 (from thermal decomposition of ammonium vanadate) and Cr_2O_3 (from thermal decomposition of ammonium dichromate). Samples were heated in a stepwise manner up to 973 K. The presence of a single phase was checked by XRD analysis.

TPR and TG measurements were carried out in a reactor fed with a H_2 (10%)/N_2 stream. The temperature was raised up to 1273 K at a heating rate of 5 K min^{-1}. The sample weights were set at $\sim$50 mg (TPR) and $\sim$20 mg (TG). For TPR the hydrogen consumed was detected by a thermal conductivity cell. To study the reverse reaction, the reduced sample at the end of the TPR or TG run (1273 K) was reoxidized in air in the TG apparatus at the same heating rate up to different temperatures (623, 673, 723, 798, and 1073 K). After each run the sample was analyzed by XRD and IR, and the TG pattern for the last two runs was recorded.

XRD spectra were obtained on a Phillips PW 1714 diffractometer with Cu$K\alpha$ (Ni-filtered) and Co$K\alpha$ (Fe-filtered)

[1] To whom correspondence should be addressed.

0022-4596/99 $30.00

radiations. Cell parameters were refined by means of the PIRUM program of Werner (7).

IR spectra were recorded with a Perkin Elmer 580 B spectrometer using the KBr pellet technique.

ESR spectra were recorded at room temperature (RT) and at 353 and 77 K on a Varian E-9 spectrometer (X-band) equipped with an on-line computer for data treatment. The absolute concentration of the paramagnetic species, N, was determined from the integrated area of the spectra, using as standards two pure copper compounds, namely, $CuSO_4 \cdot 5H_2O$ and $Cu(acac)_2$ (Cu-acetylacetonate), and using the equation

$$N_a = N_b \cdot \frac{g_b}{g_a} \frac{S_b(S_b + 1)}{S_a(S_a + 1)} \cdot \frac{A_a}{A_b}, \qquad [1]$$

where As are the integrated areas (measured at the same temperature), g is the g value, S is the spin, and a refers to the sample and b to the standard.

Samples were also analyzed by SEM microscopy in a Phillips 505 electron microscope with an EDAX 9100 microprobe with an energy dispersive detector.

RESULTS AND DISCUSSION

The TPR pattern of the $CrVO_4$ phase shows two intense and consecutive peaks of similar intensity reaching maximum at 833 and 887 K (Fig. 1a). The V_2O_5 reduction profile, recorded under similar conditions, is included for comparison (Fig. 1b).

TPR studies have amply shown that the $V^V \rightarrow V^{III}$ reduction of V_2O_5 depends on the experimental conditions. It is a multistep process with the clear formation of the VO_2 intermediate phase (8, 9). This phase occurs at ~ 923 K, whereas from 1023 K the stable oxide is V_2O_3 (10).

Considering that V^V is the unique reducible species of the $CrVO_4$ phase, the TPR signals of Fig. 1a can be formally assigned to the $V^V \rightarrow V^{IV} \rightarrow V^{III}$ stepwise processes. In V_2O_5 after TPR at ~ 940 K, XRD detected the presence of VO_2, but also at temperatures lower than 940 K the presence of V^{III} cannot be excluded. The sharp signal of the second reduction step (887 K) is diagnostic of a higher reducibility of the V^{IV} species of the $CrVO_4$ phase. Differences in the reducibility could depend partly on the structural characteristics of $CrVO_4$ (i.e., tetrahedral vanadate species, availability of oxygen atoms) but mainly on the higher dispersion of the reducible vanadium owing to the presence of chromium. The suggested V^{IV} intermediate phase at ~ 840 K, is less stable than that obtained from V_2O_5 under similar conditions, due to the probable incorporation of the Cr^{III} atoms in the lattice.

The TG run for the $CrVO_4$ phase, under $H_2(10\%)/N_2$ atmosphere, showed a continuous weight loss variation that started at 713 K, reached 93% reduction at 873 K and

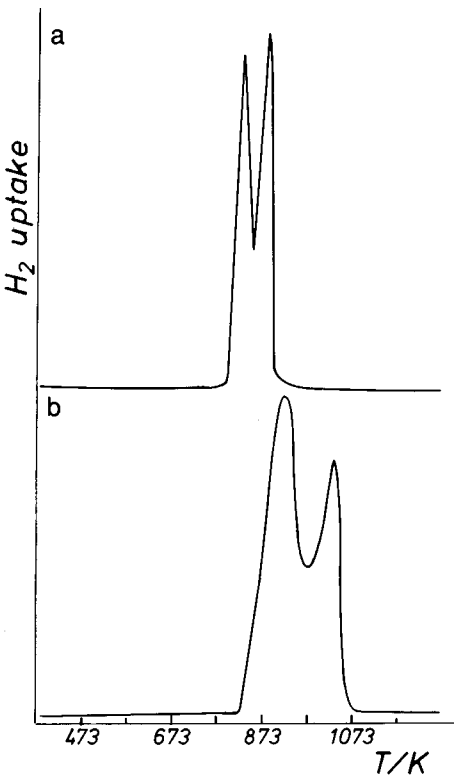

FIG. 1. Temperature programmed reduction pattern of (a) $CrVO_4$ and (b) V_2O_5.

a 9.55% weight loss at 1273 K, in agreement with the expected loss (9.58%). Thus, unlike the TPR pattern, the TG pattern did not resolved into a two-step process. The two results do not necessarily conflict because the underlying mass transport processes differ. Whereas the H_2 adsorbed, monitored by TPR, gives information about the nature of the adsorption site as well as the kinetics of vanadium reduction, TG measures the weight change due to the desorption of water. On oxidic systems, the H_2 can be adsorbed at low temperatures without a complete release of water because the hydrogen ions form OH^- species that can diffuse into the lattice, mainly into the rutile-like or disordered structures.

Because low temperatures yielded amorphous samples, XRD measurements failed to clarify the first stages of the reduction process. However, XRD at ~ 800 K inferred the formation of a rutile-type structure and did not detect free Cr_2O_3 oxide. Efforts to improve crystallinity by decreasing the heating rate to 2.5 K min^{-1} proved unsuccessful.

Although the post-TPR 900 K sample still had poor crystallinity, it improved after continuous heating in H_2/N_2 atmosphere up to 1050 K. The XRD pattern revealed the presence of a $CrVO_3$ corundum-like phase. The observed cell parameters $a = 4.98(2)$ Å and $c = 13.76(3)$ Å were in good agreement with reported values (2).

The ESR spectra for the original sample and for post-TPR 843 and 1073 K samples, recordered at three temperatures (353 K, room temperature, and 77 K) showed a symmetrical Lorentzian line centered at $g = 1.97$ (Fig. 2). At 353 K and at room temperature (RT) the linewidth (ΔH_{pp}) was 150–170 G, and as the recording temperature was lowered (77 K) the linewidth increased ($\Delta H_{pp} =$ 360–400 G). The spectra were recorded at 353 K, a temperature higher than the Neel temperature of α-Cr_2O_3 ($T_N = 308$ K). Above T_N α-Cr_2O_3 gives a single symmetrical line at $g = 1.97$ ($\Delta H_{pp} = 480$–500 G), whereas below T_N it is ESR silent (11). The absence of a broad signal with this linewidth (Fig. 2d) permits us to exclude the presence of the free α-Cr_2O_3 oxide in our reduced samples. The α-Cr_2O_3 spectrum, recorded at 353 K, is also included for comparison (Fig. 2e).

From the integrated intensity of the spectra recorded at RT we obtained the following absolute concentration of Cr^{III} (10^{21} ions/g): 1.8 for original sample, 1.0 for post-TPR 843 K sample, and 0.05 for post-TPR 1073 K sample, namely, in the ratio 100:54:3. Because the theoretical Cr^{III} concentration in the untreated $CrVO_4$ is 3.6×10^{21} ions/g, ESR yielded only 50% of the nominal value. Despite the large possibility of errors in the determination of absolute spin, we believe that this difference is reliable and arises from the relatively high T_N value (50 K) (12) of the orthorhombic $CrVO_4$ phase, which invalidates the simple Curie law. Evidence arguing in favor of the nonvalidity of the Curie law and the occurrence of the more general Curie–Weiss law is the ratio of the integrated intensities at 77 K and at RT, (A_{77}/A_{RT}). Whereas the $CuSO_4$ $5H_2O$ standard sample had an A_{77}/A_{RT} ratio of 3.5, *i.e.*, near to the theoretical value of 3.8, the original and post-TPR 843 K samples had lower values (1.9–2.5).

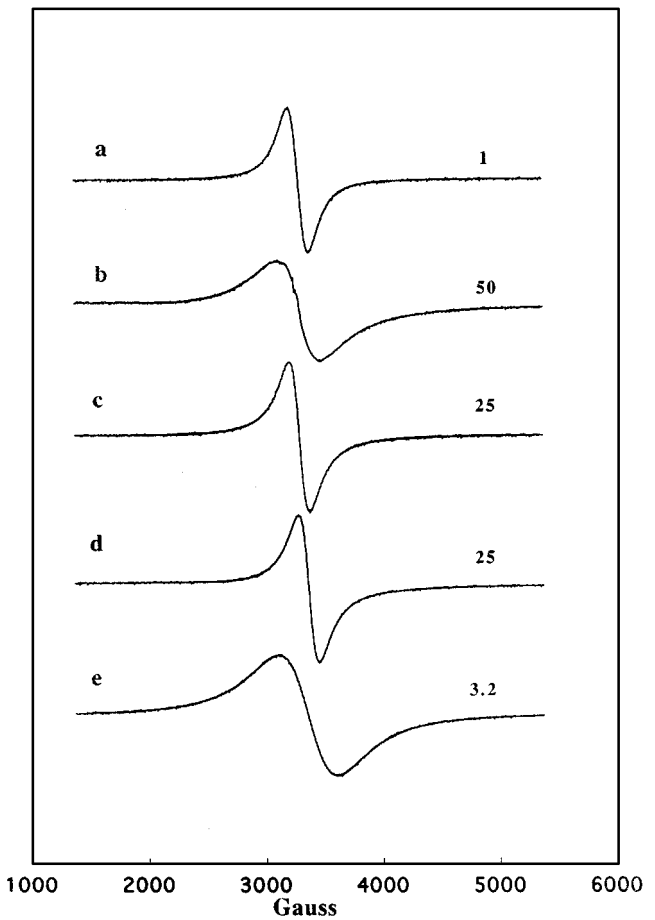

FIG. 2. ESR spectra of $CrVO_4$ original sample, recorded at RT (a); $CrVO_4$ TPR at 1073 K, recorded at 77 K (b), at RT (c), and at 353 K (d); and α-Cr_2O_3, recorded at 353 K (e). The figure on each spectrum indicates the relative gain.

The ESR signals of the sample before and after TPR had similar features (g value, lineshape, linewidth, and linewidth dependence on the recording temperature), differing only in their relative intensity. These findings suggest a common assignment, namely, to exchange-coupled Cr^{III} ions in the $CrVO_4$ crystalline and/or a disordered phase because reduction at low temperatures produced an amorphous sample.

The IR spectrum of $CrVO_4$ was consistent with the presence of VO_4^{3-} groups in C_{2v} symmetry sites (intense V–O stretching bands at 910, 870, 715 cm^{-1} with a shoulder at $\sim$660 cm^{-1}, Fig. 3a (13)). A second group of split bands between 500 and 300 cm^{-1} is attributed to the bending modes of the tetrahedral groups, including also the CrO_6 vibrations (13), with an important coupling effect between both type of polyhedra. On the other hand, whereas α-Cr_2O_3 presented the typical spectrum containing two intense IR bands at 623 and 565 cm^{-1} (Fig. 3d), the α-V_2O_3 phase, like the VO_2 oxide, showed very poor resolution (Fig. 3e). These lower vanadium oxides invariably yield only weak or very weak signals in the 700–550 and 650–500 cm^{-1} IR spectral regions (10). This behavior can be attributed to the short separations among the nearest-neighboring metallic ions with a strong t_{2g}–t_{2g} interaction. Showing a behavior between extremes of V_2O_3 and Cr_2O_3, the IR spectrum of $CrVO_3$ (Fig. 3c) showed intense bands at 593 and 546 cm^{-1}, with a shoulder at 492 cm^{-1}. Some other bands of lower intensity (419 vw, 385 m, 302 vw, and 278 vw) can be assigned to the bending and lattice modes. The two spectral features that distinguish the V_2O_3 and Cr_2O_3 spectra were the slight shifting of the bands and their intensities related to the structural and to the V^{III} and Cr^{III} characteristics (including size and electronic configuration). The c/a parameter ratio and cell volume of the $(Cr_{1-x}V_x)_2O_3$ solid solution do not follow Vegard's law in the complete range of composition (only between Cr_2O_3 and $Cr_{0.04}V_{1.96}O_3$) (12, 14). In addition, the V_2O_3 lattice is relatively smaller than that expected (2), according to the ionic radii: $r_{V^{III}} = 0.64$ Å and $r_{Cr^{III}} = 0.615$ Å (15). This difference is reflected by a slight reinforcement of the V–O

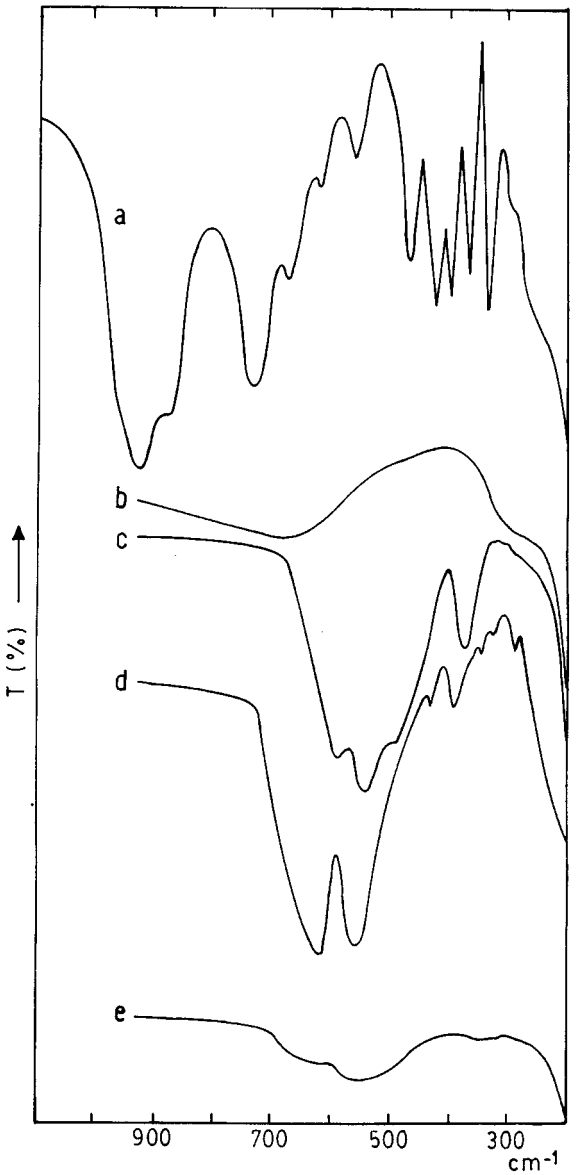

FIG. 3. IR spectra of (a) $CrVO_4$ original sample; (b) $CrVO_4$, TPR 843 K; (c) $CrVO_4$, TPR 1073 K; (d) α-Cr_2O_3; and (e) α-V_2O_3.

vibration accompanied by a marked decrease in the band intensities. However, incorporation of the Cr in the lattice enhanced the separation of the nearest-neighboring vanadium atoms, thus improving the resolution of the IR spectra. Hence, these IR spectroscopic features may directly depend on the structural and electronic properties of $CrVO_3$. A similar behavior has been observed in the TiO_2–V_2O_5 reduced system, where Ti stabilizes V^{IV} thereby also improving the resolution of the IR spectrum (16).

SEM microscopy specified the morphology of the crystal showing that the original $CrVO_4$ (orthorhombic phase) differed from the intermediate phase (with prismatic crystals similar to those observed for VO_2 rutile structure) (17) and from the final $CrVO_3$ product belonging to the hexagonal crystal system (Fig. 4). Note that microprobe analysis determined similar Cr and V contents in all samples.

To investigate the intermediate phase, suggested by TPR, XRD, and SEM and scarcely by IR (but not by TG or ESR), we studied the reverse reaction from $CrVO_4$ to $CrVO_3$. The TG run stopped at 1073 K (not reported) showed a continuous weight increase from $\sim$573 to $\sim$893 K, and then no further variation up to 1073 K. The average weight increase over three runs ranged from 8.38–9.60%. This corresponds to 80–90% of the theoretical value for the oxidation from $CrVO_3$ to $CrVO_4$, indicating an almost complete reversibility of the reaction. The run stopped at 798 K gave a weight increase of 5.05% as expected for the formation of the intermediate phase (50% of the total value for the complete oxidation).

IR and XRD spectra for the samples after TG runs at different temperatures are shown in Fig. 5. The IR spectra gave the best evidence of the formation of an intermediate phase containing V^{IV}. The post-TG 623 K sample (Fig. 5a) and the post-TG 1073 K sample (Fig. 3c) had substantially identical IR spectra (intense bands at 593 and 546 cm^{-1}). They differed only in a slight broadening of the bands of $CrVO_3$ bands. In the post-TG 673 K and post-TG 723 K samples these bands progressively broadened and weakened and new weak bands appeared (1014 and 880 cm^{-1} in Fig. 5b and 1018, 930 and 860 cm^{-1} in Fig. 5c).

The IR spectrum of the sample treated up to 798 K (Fig. 5d) differed markedly from the previous spectra: the $CrVO_3$ bands practically disappeared and new and relatively intense bands appeared at 720, 641, and 531 cm^{-1}. Likewise, bands at higher wavenumbers already present in the spectrum of the post-TG 723 K sample (Fig. 5c) were reinforced and showed small shifts (1023, 942, and 869 cm^{-1}).

The higher region of the spectra can be assigned to V^{V}–O stretching modes: bands at 942–869 cm^{-1} are related to $CrVO_4$ (see Fig. 3a), whereas those observed at the highest wavenumbers (1014–1023 cm^{-1}) are typical of the shortest V = O bond of V_2O_5 (10). They can be due to the few capping vanadium atoms present on the surface, which are the most sensitive to oxidation. Bands located in the intermediate region of the spectrum (720, 641, and 531 cm^{-1}) correspond to V^{IV}–O stretching modes, whereas the bands of V^{III}–O and Cr^{III}–O stretching are observed in the region below 650 cm^{-1}. This region is also typical of the O–V^{IV}–O and O–V^{V}–O bending modes (10).

Although the XRD spectra (shown in Fig. 5) indicated that the samples were largely amorphous, the broad, weak peaks suggested the presence of some phases: the XRD pattern of the post-TG 623 K sample (Fig. 5e) revealed the presence of the $CrVO_3$ corundum-like phase. These peaks were also present (but at reduced intensity) in the spectrum

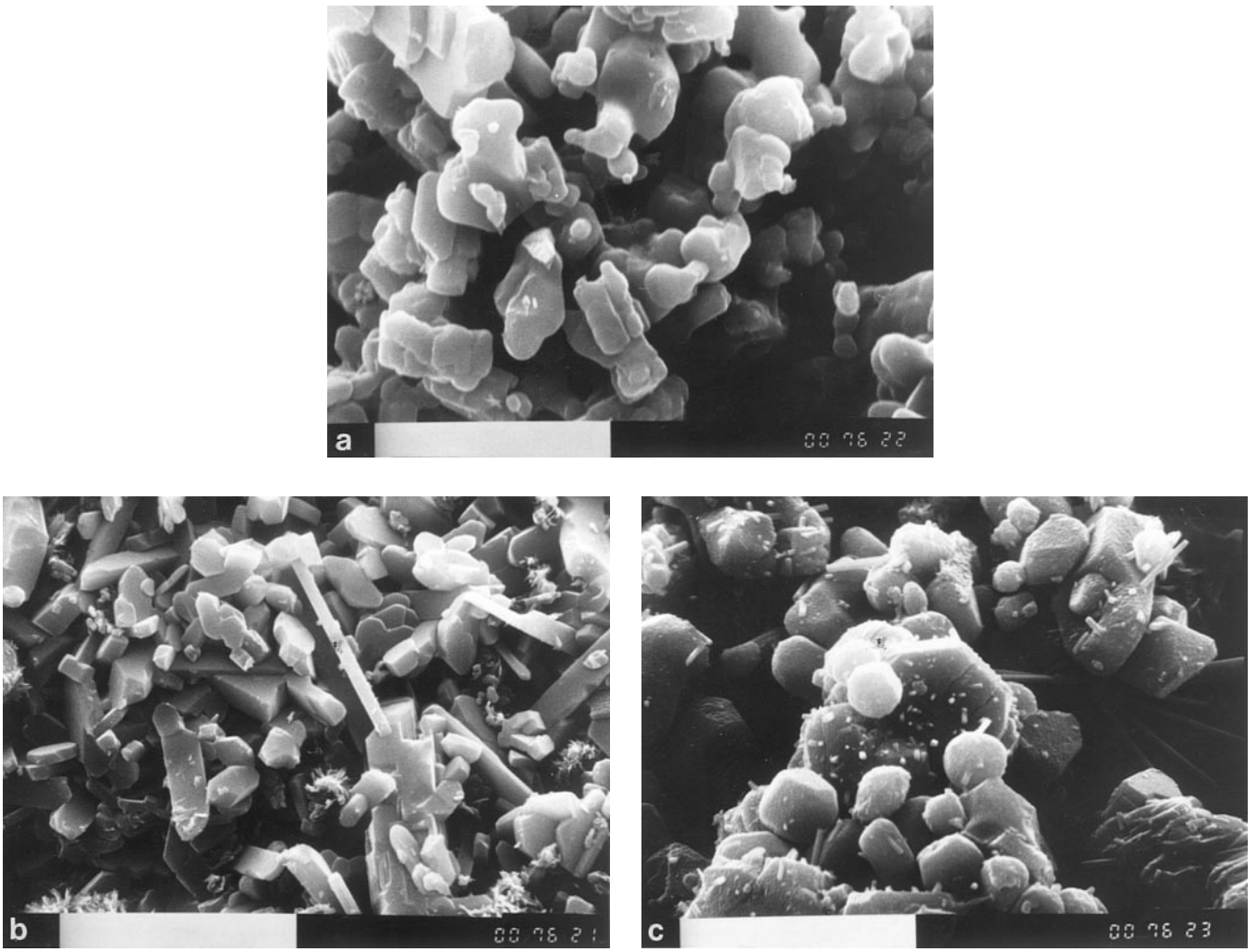

FIG. 4. Micrographs (magnitification, $\times 5000$, scale bar = 10 μm) of (a) $CrVO_4$; (b) $CrVO_4$, TPR 843 K; and (c) $CrVO_4$, TPR 1073 K.

of the post-TG 723 K sample (Fig. 5f), which also revealed some other very weak peaks. In the last spectrum (Fig. 5g, 798 K) the $CrVO_3$ peaks almost disappeared and the others strengthened: among these one of the most intense is that at $2\Theta = 32.5^\circ$, attributable to a rutile-like phase ($2\Theta = 32.47^\circ$ for VO_2 (18)).

The absence of free α-Cr_2O_3 in all reduction steps (shown by ESR and IR) and the good reversibility of the reaction indicated that the intermediate phase was not pure VO_2 but a related phase containing V^{IV} and Cr^{III} ions, analogous to that formed in the TiO_2 (rutile)–Cr_2O_3 (corundum) system. In this system the presence of Wadsley intergrowth defects forms arrangements of alternating blocks of rutile–corundum (*reduced rutile*) structures because both lattices can be described as a close packing of oxygen (19–21). In our system the smaller range of stability of the intermediate phase allows the reducing process to be continued from V^{IV} to V^{III}. Thus a small increase in the temperature prevents the growth of the intermediate phase crystals, giving a largely amorphous system.

CONCLUSIONS

The study of the reduction process of $CrVO_4$ by several complementary techniques has provided the following findings:

(i) The presence of α-Cr_2O_3 was excluded in all reduced samples (843 and 1073 K)

(ii) At the intermediate step of the reduction process (843 K) the incorporation of Cr^{III} in a VO_2 rutile phase has been suggested. The best evidence of the formation of this phase arose from the study of the reverse reaction.

(iii) The species observed from ~ 878 K was V^{III} in a corundum-type $CrVO_3$ mixed oxide.

(iv) Differences in the resolution and intensity of the IR bands of V_2O_3 and $CrVO_3$ can be related to structural and electronic properties.

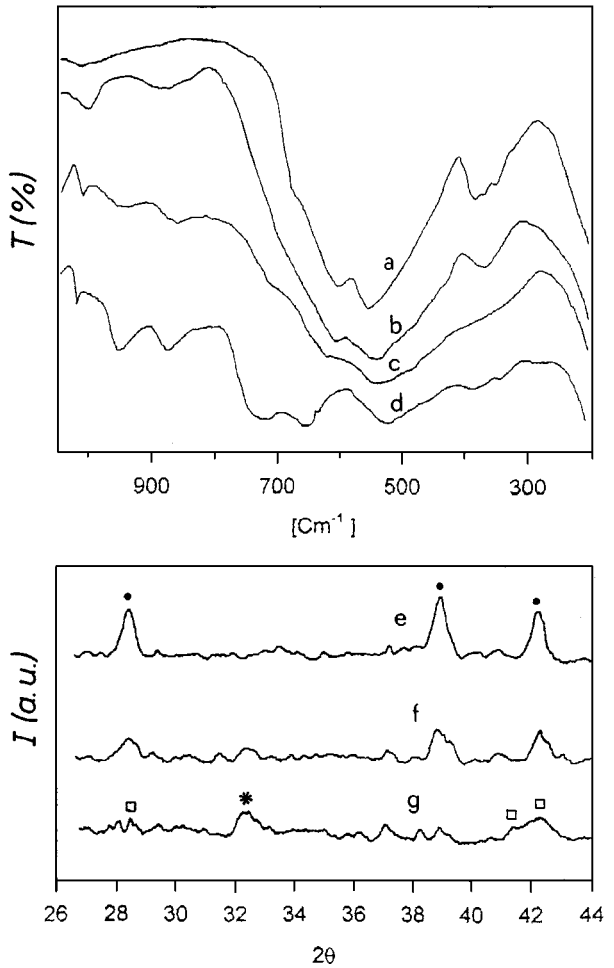

FIG. 5. (Top) IR spectra of $CrVO_4$ reduced at 1073 K and reoxidized in air by TG stopped at different temperatures: (a) 623 K, (b) 673 K, (c) 723 K, and (d) 798 K. (Bottom) XRD spectra of the same sample reoxidized at (e) 623 K, (f) 723 K, and (g) 798 K. Circles refer to V_2O_3, asterisk to VO_2, and squares to $CrVO_4$.

ACKNOWLEDGMENTS

This work was supported by CONICET (CEQUINOR-CINDECA) (Argentina) and CNR (Italy) within the framework of the scientific agreement between the two institutions.

REFERENCES

1. E. Filipek, J. Walczak, and P. Tabero, *J. Alloys Compounds* **265,** 121 (1998).
2. A. F. Reid, T. M. Sabine, and D. A. Wheeler, *J. Solid State Chem.* **4,** 400 (1972).
3. A. F. Wells, *in* "Structural Inorganic Chemistry," p. 457. Oxford Univ. Press, London, 1962.
4. J. P. Urbach, O. Muller, E. Goering, H. Paulin, M. Klemm, M. L. den Boer, and H. Horn, *J. Phys. IV France* **7,** C2–535 (1997).
5. B. Marinder and A. Magneli, *Acta Chem. Scand.* **11,** 1635 (1957).
6. D. Adler, *in* "Treatise on Solid State Chemistry" (De. N. B. Hannay, Ed.), Vol. 2, p. 237. Plenum, London, 1975.
7. P. E. Werner, *Ark. Kemi* **31,** 513 (1969).
8. A. Jones and B. McNicol, *in* "Temperature Programmed Reduction for Solid Materials Characterization," p. 113 Dekker, New York, 1986.
9. D. A. M. Monti and A. Baiker, *J. Catal.* **83,** 323 (1983).
10. I. L. Botto, M. Vassallo, E. J. Baran, and G. Minelli, *J. Mater. Chem. Phys.* **50,** 267 (1997).
11. R. Gerling and K. Drager, *Surf. Sci.* **106,** 427 (1981).
12. M. M. Schieber, *in* "Experimental Magnetochemistry: Selected Topics in Solid State Physics," (E. P. Wohlfarth, Ed.) Vol. VIII, pp. 218 and 290. North-Holland, Amsterdam, 1967.
13. E. J. Baran, *J. Mater. Sci.* **33,** 2479 (1988).
14. *X-Ray Powder Data Files*, pp. 34–187.
15. R. D. Shannon, *Acta Crystallogr. A* **32,** 751 (1976).
16. L. E. Briand, L. Gambaro, and H. Thomas, *J. Therm. Anal.* **44,** 803 (1995).
17. C. Lampe Onnerud and J. O. Thomas, *Eur. J. Solid State Inorg. Chem.* **32,** 293 (1995).
18. *X-Ray Powder Data Files*, pp. 43–1051.
19. O. W. Florke and Ch. Wang Lee, *J. Solid State Chem.* **1,** 445 (1970).
20. B. Hyde and S. Andersson, *in* "Inorganic Crystal Structures," p. 157. Wiley & Sons, New York, 1989.
21. M. O'Keeffe and T. J. Rible, *J. Solid State Chem.* **4,** 351 (1972).